Universitat Autònoma de Barcelona

[1]

Ph.D. thesis

January 2014

Searches for new physics in $t\bar{t}$ pair production at the Large Hadron Collider

Candidate
Antonella Succurro

Supervised by
Dr. Aurelio Juste Rozas
Institució Catalana de Recerca i Estudis Avancat
Institut de Física d'Altes Energies

Professore: Lei ha una qualche ambizione?

Nicola: Ma... Non...

Professore: E Allora vada via... Se ne vada dall'Italia. Lasci l'Italia finché è in tempo. Cosa vuole fare, il chirurgo?

Nicola: Non lo so, non ho ancora deciso...

Professore: Qualsiasi cosa decida, vada a studiare a Londra, a Parigi... Vada in America, se ha le possibilità, ma lasci questo Paese. L'Italia è un Paese da distruggere: un posto bello e inutile, destinato a morire.

Nicola: Cioè, secondo lei tra poco ci sarà un'apocalisse?

Professore: E magari ci fosse, almeno saremmo tutti costretti a ricostruire... Invece qui rimane tutto immobile, uguale, in mano ai dinosauri. Dia retta, vada via...

da La meglio Gioventù *di M.T. Giordana (2003)*

Introduccion

Contents

Introduction

Chapter 1

Going beyond the Standard Model

The Standard Model (SM) of particle physics is the most successful, beautyful and precise theory describing the interactions between fundamental particles. Its validity has been tested by precision measurements at the Large Electron-Positron Collider (LEP) at CERN and confirmed by the observation of all the particles it predicts, including the Higgs-like boson discovered at the Large Hadron Collider (LHC) in July of 2012 which up to now behaves as expected from the SM.

What makes the SM "only" and effective theory is the fact that unstabilities appear at high energy scales of the order of the Planck mass. In this Chapter we will show

1.1 Building the Standard Model

1.2 New Physics Models predicting vector-like quarks

[1, 2]

The ATLAS experiment at the Large Hadron Collider

The analyses presented in this dissertation have been performed analyzing data from proton-proton (p-p) collisions at the center of mass energy $\sqrt{s} = 8$ TeV recorded during the year 2012 at the ATLAS experiment [3]. In the following Chapter we will briefly describe the main features of the detector, located at the CERN laboratories in Geneva, Switzerland.

The experimental facilities are situated at Point 1 along the Large Hadron Collider (LHC) [4] 27 km long ring, shown in Figure 2.1. The accelerator tunnel can reach an underground depth of 175 meters and is spread between Swiss and French territory, while the cave where ATLAS is allocated is about 100 meters underground in the CERN Swiss site of Meyrin.

The LHC program was approved by CERN Council in 1994, followed by the approval of the four main experiments physics programs: ATLAS [3] and CMS [5] in 1996; ALICE [6] in 1997; LHCb [7] in 1998. Works towards the installation of the most powerful particle accelerator of the world started when the Large Electron Positron Collider (LEP) was dismantled in 2000 to give up its place in the tunnel to the LHC, which was then fully operational by 2008.

The LHC is composed of eight arcs 2.7 km long, each of which contains 154 dipole magnets, whose function is to bend the beams along the circular trajectory, and 49 quadrupole magnets, that focus the beam. These superconducting magnets operate at a temperature of 1.9 K, maintained by means of liquid Helium vessels. Eight insertions are placed inbetween the arches. Each insertion has a specific role that characterizes its design and can be injection, beam dumping, beam cleaning, or "physics", i.e. make the beams collide within an experiment.

First proton beams were circulated on 10th September 2008 and right on the verge of getting the first collisions at a center of mass energy $\sqrt{s} = 900$ GeV nine days later, an electrical connection joining superconducting wires of a dipole and a quadrupole failed. This caused the release of liquid Helium in the insulating vacuum, resulting in an explosion that severely damaged the machine. After more than one year devoted to repair the damage

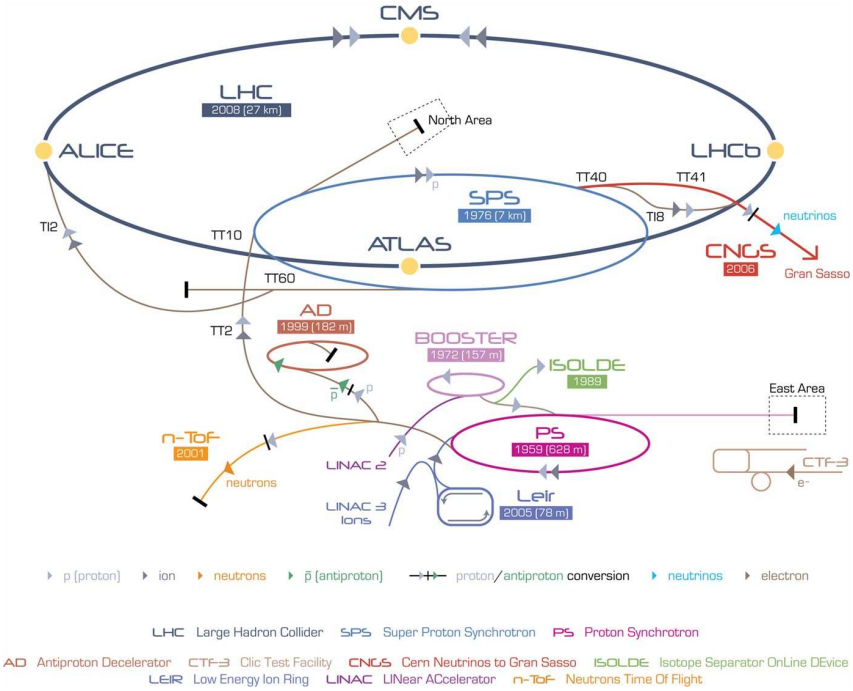

Figure 2.1: A schematic showing the accelerator complex at CERN. Protons are extracted from Hydrogen gas and injected in the first machine, the linear accelerator LINAC2 that starts the acceleration chain. When protons reach an energy of 50 MeV they are injected into the Proton Synchrotron Booster (PSB) and accelerated up to the energy of 1.4 GeV. The second circular accelerator, the Proton Synchrotron (PS) brings the energy of the protons to 25 GeV previous to injecting them into the last machine before the LHC, the Super Proton Synchrotron (SPS). Protons of 450 GeV finally enter the LHC where they are boosted to energies of up to 4 TeV. The four main LHC experiments are shown on the collider ring.

and consolidate the security, on 30th November 2009 the LHC became the world's highest energy particle accelerator[1]:

> Geneva, 30 November 2009. CERN's Large Hadron Collider has today become the worlds highest energy particle accelerator, having accelerated its twin beams of protons to an energy of 1.18 TeV in the early hours of the morning. This exceeds the previous world record of 0.98 TeV, which had been held by the US Fermi National Accelerator Laboratorys Tevatron collider since 2001. It marks another important milestone on the road to first physics at the LHC in 2010.

The main performance figure of merit for an accelerator is the luminosity, the instantaneous luminosity $\mathcal{L}$ being defined as

$$\mathcal{L} \times \sigma = \frac{dN}{dt} = f \times n \frac{N_1 \times N_2}{A} \times \sigma. \tag{2.1}$$

Here dN/dt is the event rate of a certain process and σ is its cross section. This rate is directly proportional to the the frequency f, the number of bunches n and the number of particles in the two bunches N_1, N_2, and inversely proportional to the beam cross-section A.

[1] http://press.web.cern.ch/press/PressReleases/Releases2009/PR18.09E.html

Parameter	designed	2010	2011	2012
Beam energy (TeV/c)	7	3.5	3.5	4
Beta function $\beta*$ (m)	0.55	2.0/3.5	1.5/1.0	0.6
Max. No. bunches/beam	2808	368	1380	1380
Max. No. protons/bunch	1.15×10^{11}	1.2×10^{11}	1.45×10^{11}	1.7×10^{11}
Bunch spacing (ns)	25	150	75/50	50
Peak luminosity ($\mathrm{cm^{-2}s^{-1}}$)	1×10^{34}	2.1×10^{32}	3.7×10^{33}	7.7×10^{33}
Emittance ε_n (μrad)	3.75	2.0	2.4	2.5

Table 2.1: Overview of some parameters for the LHC performance comparing the design values with their time evolution during the first long run operation in 2010-2013 [8].

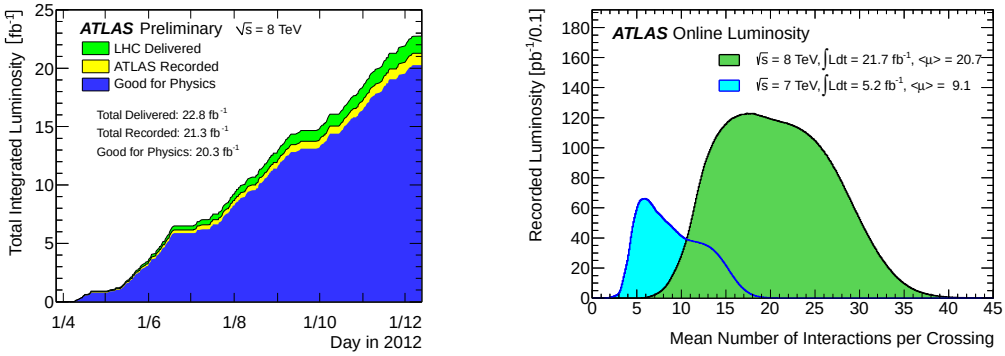

(a) (b)

Figure 2.2: (a) Total integrated luminosity versus time delivered by the LHC to ATLAS (in green), recorded by the experiment (in yellow) and selected as "good data" for analysis (in blue) for p-p collisions at $\sqrt{s}$=8 TeV. (b) Mean number of interactions per beam crossing during 2011 and 2012 LHC runs, where $\mu = \mathcal{L} \times \sigma_{\mathrm{inelastic}}/f$ depends on the instantaneous luminosity $\mathcal{L}$, the p-p inelastic cross section $\sigma_{\mathrm{inelastic}}$ and the revolution frequency f. [9]

Integrating over the accelerator active time (a "fill", when stable beams are kept colliding) gives the *integrated luminosity*, relating the total number of produced events N_{tot} to the cross-section:

$$\int \mathcal{L}dt = \frac{N_{tot}}{\sigma}. \tag{2.2}$$

In 2012 LHC reached a peak luminosity of 7.7×10^{33} $\mathrm{cm^{-2}s^{-1}}$ which is more than half the design luminosity, as shown in Table 2.1 together with other parameters relevant for the accelerator performance. Over the last year of data taking before the long shutdown[2] ATLAS collected about $20\mathrm{fb}^{-1}$ of p-p collision data at $\sqrt{s}$=8 TeV. Figure 2.2(a) shows the delivered luminosity from the start of stable beams until beam dump and the luminosity recorded by ATLAS during stable beam conditions, the difference with respect to the delivered luminosity being due to Data AQuisition (DAQ) inefficiencies. Of the recorded luminosity, only a part

[2]LHC terminated the p-p program at the end of 2012, operated proton-heavy ion collisions for two months at the beginning of 2013 and then stopped for what is called the first long shutdown. During this two-years time the accelerator and the experiments as well will undergo substantial maintenance and upgrade works, in order to be re-operated in 2015 with higher performance at a higher center of mass energy for particle collisions.

is usable for analysis, and is what is called "good data", i.e. the data that satisfy Data Quality (DQ) requirements assessed after reprocessing.

In order to increase the luminosity LHC operates with higher number of protons per bunch as well as higher number of bunches per beam and reduces the inter-bunch latency time. This overall defines a set of challenges that physics analysis will face associated to the high luminosity. Even at the detector design stage, the high frequency of collision environment foreseen influenced the choice of radiation resistance material for the experiment sub-systems. Concerning directly the physics instead we can list the main problematics as being *underlying events* and *pile-up*

Underlying events are the product of the hadronic character of p-p hard interaction, where the main collision process is accompanied by secondary parton interactions at low transfered momentum (soft QCD) and are flavor- and color-connected to the hard scattering. They are observed as jets of particles close to the direction of the beam and are in general not separable from the event of interest. Their contribution can be studied with Monte Carlo techniques tuned with data from *minimum bias* events, as perturbative theory does not properly model low momentum QCD.

Pile-up events are distinguished between *in-time* and *out-of-time* pile-up. The first ones come from the multiple inelastic scatterings of protons in the same bunch, as if we consider a cross-section of 80 mb at the nominal luminosity of 10^{34} cm^{-2}s^{-1} the number of events per second will be something like a billion. This translate, at a collision frequency of one crossing every 25 ns, to about 20 interactions per crossing that will be detected simultaneously. On the other hand, the inter-bunch time interval is so short that the electronics reading the detector might not keep up with the frequency of collisions, leading to the cumulation of events that happened in different beam crossings.

ATLAS makes use of a three-level trigger system (described in Section 2.1.6) to identify and record only the events of interest, while the pile-up issues are dealt with at the analysis reconstruction level.

2.1 The ATLAS detector

ATLAS (A Toroidal LHC ApparatuS) [3] is a general purpose experiment aimed at exploring a vast range of physics scenarios. It is characterized by a full coverage of the space around the p-p interaction point and complete containment of the particles produced in the collision. Different subsystems are layered concentrically one after the other, each of them pursuing a specific task. Right around the interaction point (IP) where the LHC makes protons collide there is the Vertex Detector, reconstructing charged particles trajectories that are bended by the first solenoid magnet surrounding the Vertex Detector. Particles going through it then encounter the two calorimeter systems, the Electromagnetic and the Hadronic one. Muons are the only particles that will pass the calorimeters material (beyond neutrinos) and a dedicated Muon Spectrometer is the last piece of detector, embedded in a huge toroidal magnet. The detector complex is presented as a schematic in Figure 2.3.

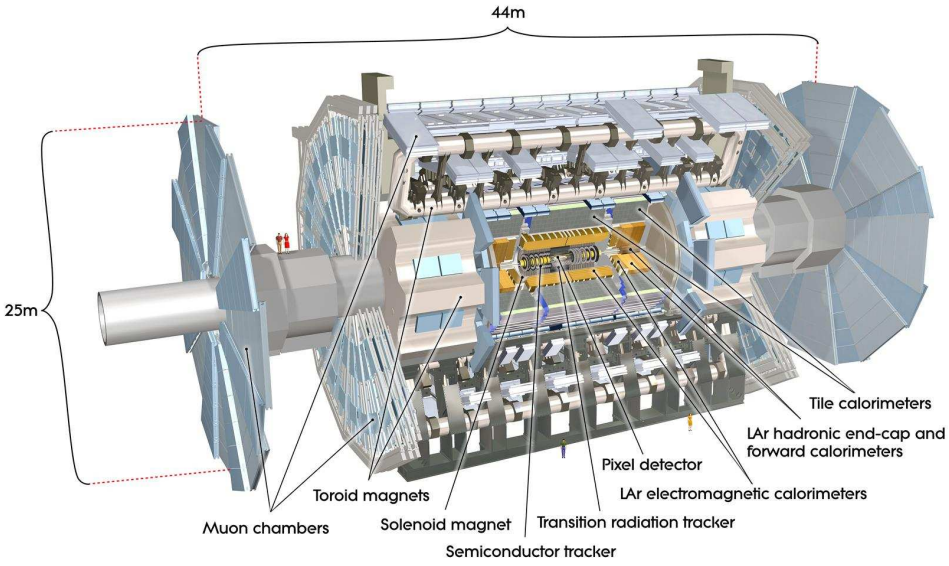

Figure 2.3: Schematic drawing of the ATLAS experiment. The detector subsystem are indicated as well as the total dimensions.

2.1.1 Coordinate system

Protons from the two circulating beams are made to collide in the center of the ATLAS detector, in the region that takes the name of Interaction Point (IP). The IP is taken as the origin of a three dimensional XYZ right-handed coordinate system. The Z axis is tangent to the trajectory of the beams while the XY plane is perpendicular to it and defines a symmetry plane for the detector, dividing it into the A and C sectors, respectively in the positive and negative Z semi-axes. Figure 2.4(a) shows a schematic of the coordinate system.

In terms of polar coordinates, the Z axis is again along the beam axis and in the transverse plane the R and ϕ coordinates are defined with ϕ ranging between $-\pi$ and $+\pi$ with respect to the X axis. In terms or spherical coordinates (see Figure 2.4(b)), the radial vector R originates from the IP, the azimuth ϕ is the same as the polar angle ϕ, and the polar angle θ is measured with respect to the Z axis and ranges between 0 and π.

Since the interaction initial energy is unknown, being dependent on the parton distribution functions for the proton energy, it is useful to define the transverse component of variables of interest[3] like the energy and the momentum, being taken as the projection on the XY plane:

$$E_{\mathrm{T}} = E \sin\theta, \qquad p_{\mathrm{T}} = p \sin\theta. \tag{2.3}$$

Another common variable used at hadron colliders to describe the polar distribution and

[3]These quantities transverse initial value will be, indeed, zero, as the protons are accelerated along the Z axis.

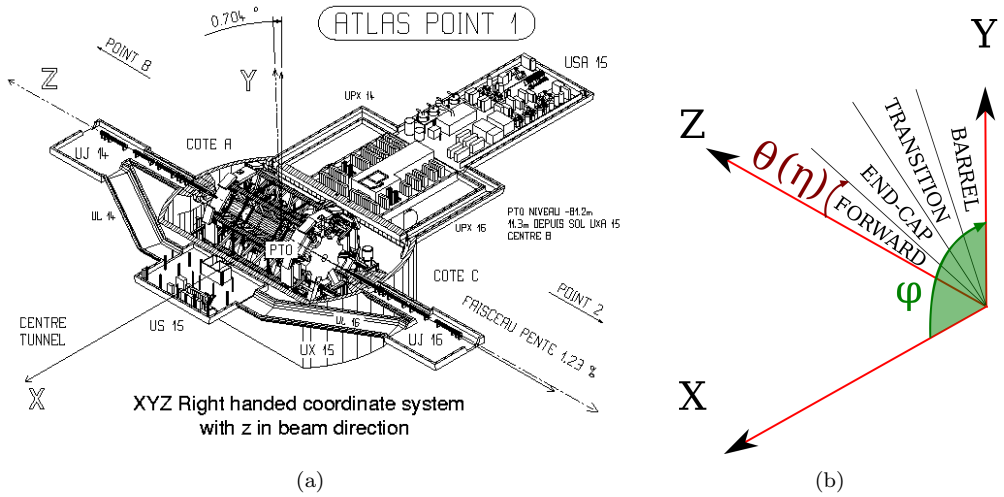

(a) (b)

Figure 2.4: (a) Drawing of the ATLAS experiment with the cartesian coordinate system. The positive X axis points towards the center of the LHC ring. The positive Z axis points todards the circulating direction of beam 2. (b) Simple schematic showing the spherical coordinates and the region definition in terms of the absolute value of the pseudorapidity η. These regions are symmetrical with respect to the transverse XY plane.

preferred to the simple polar angle θ is the pseudorapidity η:

$$\eta \equiv -\ln\left(\tan\frac{\theta}{2}\right); \tag{2.4}$$

which, for relativistic regimes, is equal to the rapidity y:

$$y \equiv \frac{1}{2}\ln\left(\frac{E+p_Z}{E-p_Z}\right); \tag{2.5}$$

and Δy and $\Delta\eta$ are Lorentz invariant. The pseudorapidity is preferred to the rapidity as it does not require knowing the particle mass but only its polar position. The distance between two particles is often referred to in terms of ΔR:

$$\Delta R = \sqrt{\Delta^2\eta + \Delta^2\phi}. \tag{2.6}$$

Figure 2.4(b) shows how different pseudorapidity regions are named. Particles along the Z axis have a pseudorapidity $|\eta| = \infty$, particles along the Y axis have a pseudorapidity $|\eta| = 0$. ATLAS has an excellent hermeticity and is able to cover pseudorapity regions up to $|\eta| = 4.9$. Typically, physics analysis consider objects in the pseudorapity region $|\eta| < 2.5$. For a quick visualization of the correspondence in terms of polar angle distribution, some pseudorapidity values are reported in Table 2.2.

θ	0°	5°	10°	20°	30°	45°	60°	80°	90°
η	∞	3.13	2.44	1.74	1.31	0.88	0.55	0.175	0

Table 2.2: Pseudorapidity vs polar angle values.

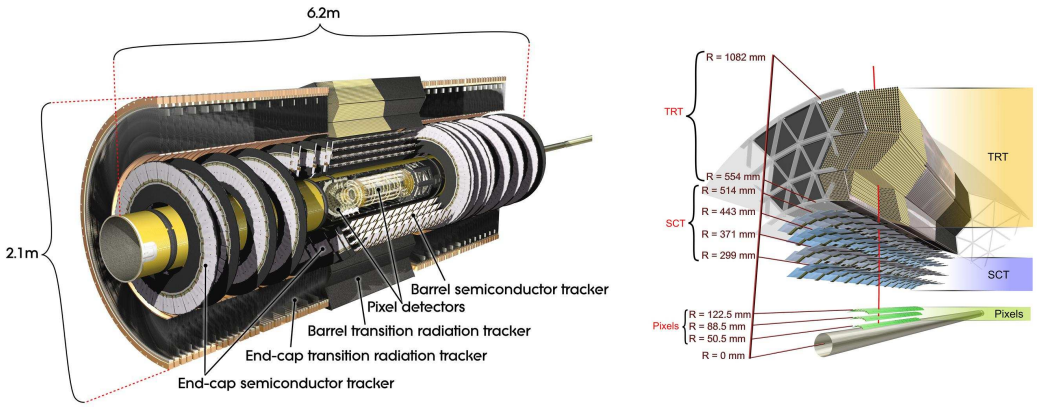

(a) (b)

Figure 2.5: (a) Schematic of the ID system. (b) Detailed schematic of the barrel section of the ID showing the three subsystems and reporting the distance to the center of the beam pipe.

2.1.2 Magnets

ATLAS is provided with four superconducting magnets that allow the measurement of charged particles momenta by curving their trajectory.

A central solenoid sits around the inner detector and produces a 2 T magnetic field along the direction parallel to the beam axis. It is only 45 mm thick (equivalent to 0.66 radiation lenghts X_0) and is cooled with liquid Helium, sharing the cryostat with the electromagnetic calorimeter.

Three toroidal magnets, one in the barrel region and the other two in the end-cap regions, produce a magnetic field of 0.5 T and 1 T respectively in the direction orthogonal to the muons trajectory.

2.1.3 Inner detector

The Inner Detector (ID) is the subsystem closest to the IP and tracking charged particles arising from collisions allows for the measurement of their momentum and vertex reconstruction with excellent resolution. At the design choices level, radiation resistance had to be taken into account, as well as reducing the amount of material to be placed in front of the calorimeters to avoid spoiling the energy measurement. This quantity varies between 0.5 and 2.5 X_0 depending on the pseudorapidity region, most of it coming from supporting equipment. This material is responsible for photon conversions and electron bremsstrahlung.

The ID is surrounded by the central solenoid magnet (Section 2.1.2) and is composed by three subsystems, from the closest to the furthest from the IP: a pixel detector, a silicon strip detector and a straw detector (Figures 2.5(a) and 2.5(b)).

Silicon Detectors

The first subsystem covers the region $|\eta| < 2.5$ and is composed by three cylindrical layers in the barrel region, each of them distant from the beam by 50.5 mm, 88.5 mm and

122.5 mm respectively, and by three concentric discs in the end-cap region, each of them distant from the beam by 49.5 mm, 58.0 mm and 65.0 mm respectively. Each silicon pixel has a size of 50×400 μm^2 and is 250 μm thick, with in total ∼80.4 million readout channels to achieve a very fine granularity. The precision is of 10 μm in $R\phi$ and 115 μm in Z and R in the barrel and end-cap region respectively.

The very first layer is called $B-$layer as, thanks to its position really close to the IP, allows for the reconstruction of secondary vertices associated with the production of short lived particles such as $B-$hadrons. This information is very useful to identify particle jets from b quarks[4].

After the three layers of pixel detectors, come four layers of silicon strip detectors. The SemiConductor Tracker (SCT) also covers the region $|\eta| < 2.5$ with a barrel and end-cap design similar to the pixel detector one, being composed by eight silicon bands (two per layer) 128 mm long and 80 μm large. It makes use of ∼6.3 millions readout channels and the resolution achieved is of 17 μm in $R\phi$ and 580 μm in Z and R in the barrel and end-cap region respectively.

By allowing for four redundant position measurements[5], the SCT contributes mainly to the momentum reconstruction.

Transition Radiation Tracker

In order to reduce the amount of material in front of the calorimeters, and to reduce the construction costs as well, in the third subsystem the semiconductor technology has been substituted with straw detectors. The Transition Radiation Tracker (TRT) consists of thin proportional chambers made of straw polyimide drift tubes, 4 mm in diameter. The drift tubes are filled with a gas mixture composed of: 70% Xenon, 27% Carbon Dyoxide, 3% Oxygen. The anode collecting the electrons from the ionized gas at the passage of the charged particle is made of tungsten covered in gold.

In the barrel region the tubes are 144 cm long and placed parallel to the beam axis, while in the end-cap region they are 37 cm long and positioned radially in wheels, with layers of radiator foils alternated to layers of straws. The resolution achieved is of 130 μm in $R\phi$ and Zϕ in the two regions respectively. The covered pseudorapidity region is of $|\eta| < 2.0$ and the readout is composed by ∼351000 channels.

About 36 measurements per track are taken, and since each channel provides two independent thresholds per hit, it is possible to discriminate between electrons and pions, since the firsts will more probably reach the high threshold.

In the end, the combination of the three ID subsystems gives very precise $R\phi$ and Z measurements, as well as good track pattern recognition. The resolution on the transverse momentum, measured with cosmic muon calibration runs [10], is:

$$\frac{\sigma_{p_{\mathrm{T}}}}{p_{\mathrm{T}}} = P_1 \oplus P_2 \times p_{\mathrm{T}}, \tag{2.7}$$

where $P_1 = 1.6 \pm 0.1\%$ and $P_2 = (53 \pm 2) \times 10^{-5}$ GeV^{-1}. This means a resolution of ∼1.6%

[4] The $b-$tagging technique will be discussed in

[5] One of the coupled layers is rotated of 40mrad with respect to the other, which is parallel to the axis, giving a small stereo angle for a redundancy in the ϕ coordinate measurement.

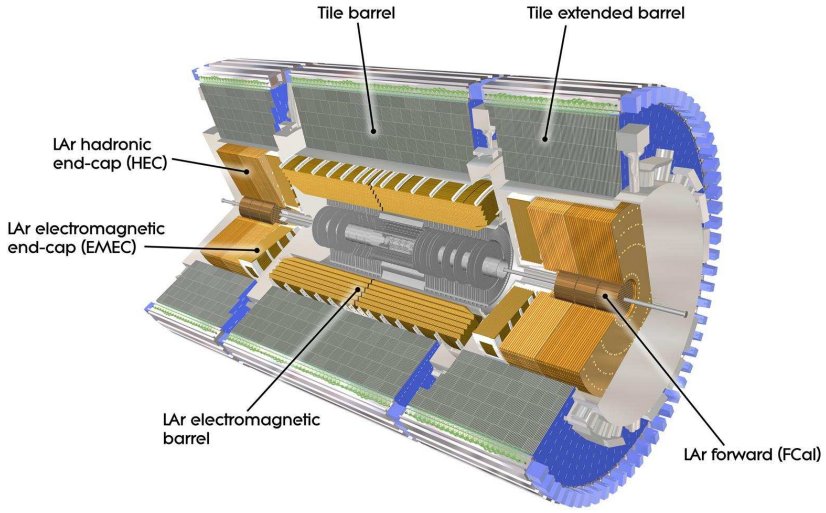

Figure 2.6: Schematic of the calorimeter complex of the ATLAS detector.

for tracks with p_{T} ∼1 GeV and ∼50% for tracks with p_{T} ∼1 TeV.

2.1.4 Calorimeters

Particles leaving the ID and surviving the crossing of the central solenoid magnet will face the calorimeter system, depicted in Figure 2.6. Different technologies are used in the barrel, end-cap and forward regions for both the Electromagnetic and the Hadronic calorimeters. The system is characterized by a coverage in pseudorapidity up to $|\eta| < 5$ and an almost full coverage in ϕ. With its 22 X_0 and 24 X_0 of material in the barrel and end-cap regions respectively it is also able to stop most of the non-muon particles from the interaction.

Electromagnetic barrel calorimeter

Electromagnetic end-cap calorimeter

Hadronic end-cap calorimeter

Forward calorimeter

Hadronic barrel calorimeter

2.1.5 Muon spectrometer

2.1.6 Trigger system

It was already introduced at the beginning of this Chapter the issue faced by LHC experiments of dealing with a huge amounts of events at very high frequencies. We remind that considering the nominal LHC luminosity of 10^{34} cm^{-2} s^{-1} a rate of interactions of

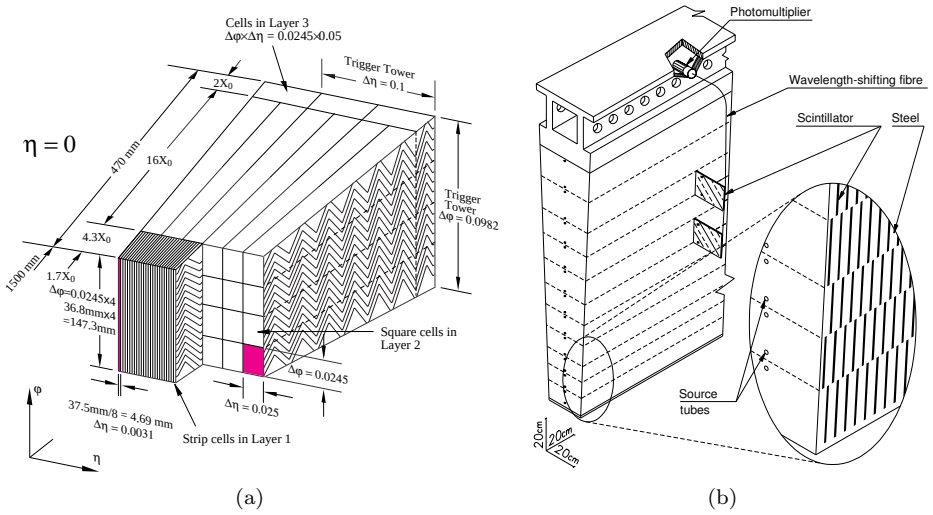

Figure 2.7: (a) Schematic drawing of a module of the Electromagnetic barrel calorimeter. (b) Schematic drawing of a module of the Hadronic barrel calorimeter.

1 GHz is expected! This poses serious technical difficulties as the maximum frequency at which data can be recorded is limited to 200 Hz considering the limited capacity for storage.

ATLAS developed a trigger system able to reduce by a factor of 10^6 the amount of data to be kept by selecting only interesting physics events. The system is divided in three levels characterized by increasing sofistication and diminishing speed. At the very first indeed we will need a really quick and simple criterium to reject useless events. The reduced information can then be processed with somehow slower logic by the other two High Level Triggers (HLT). A drawing of the system is shown in Figure 2.8.

Most of the trigger chains used for physics are un-scaled in the sense that all the events passing the selection are kept, but there are also pre-scaled trigger chains that contain either too many events or events considered not physically interesting. These trigger chains are used for checks or calibration rather than physics analysis.

Level 1 trigger

The Level 1 trigger (L1) is completely based on the hardware of the detector, taking information from calorimeters and from the muon spectrometer trigger systems RPC and TGC (Section 2.1.5) at 40 MHz (the frequency of the beam crossing) and reducing it to 75 kHz by choosing events with high transverse momentum or high missing transverse energy.

Using dedicated fast front-end electronics (the typical decision time being less than 2 μs), calorimeter cells are analogically summed to build calorimetric towers which, if having an energy higher than a certain threshold, will activate a trigger chain.

These trigger chains will then be combined with the information from the muon spectrometer to form the so-called Region of Interest (RoI) that is passed to the next trigger level.

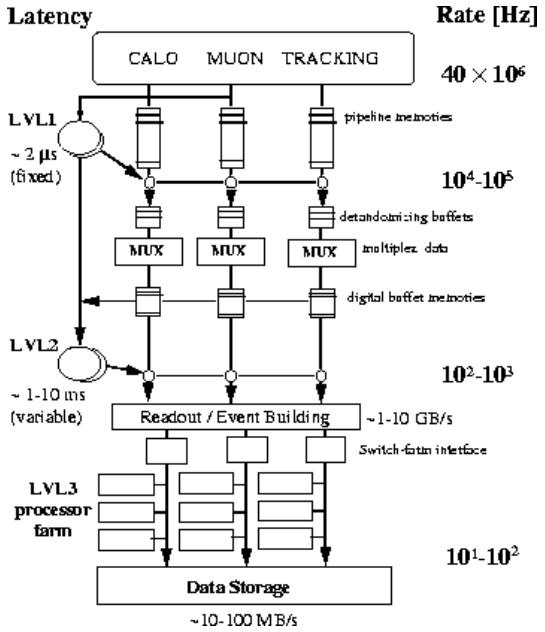

Figure 2.8: Schematic drawing of the three-level trigger system of ATLAS.

Level 2 trigger

Starting from the RoI, the Level 2 trigger (L2) will reduce the 75 kHz to 3.5 kHz of events with an average decision time of 40 ms. At this stage the information from the trackers is incorporated to the RoI to build candidate object (electrons, photons, muons) and better obtain its position and energy with simplified algorithms quick enough to respect the limit on the decision time.

Level 3 trigger

The last trigger, Level 3, is called Event Filter (EF) since at this point the physics objects are built using the same algorithms as the off-line reconstruction. With an execution time amounting to 4 s, the EF reduces the event rate to the goal value of 200 Hz.

Objects reconstruction

3.1 Electrons

3.2 Muons

3.3 Jets

3.4 Missing Transverse Energy

303 CHAPTER 4

304 Monte Carlo simulation

305 ---

306 4.1 Parton shower

307 4.2 Hadronization

308 4.3 Underlying-event

309 4.4 Generators

Chapter 5

Searches for vector-like top partner pairs in the single lepton channel

In the following Chapter we will describe two searches for vector-like top partners $T\bar{T}$ pairs performed in the single lepton channel. These analyses are optimized for different final states and are thus complementary. The first search focuses on decay channels with high BR to Wb and is performed using the full dataset of p-p collisions at the center of mass energy of $\sqrt{s}$=8 TeV collected during 2012 at the ATLAS detector, consinsting in 20.34 fb^{-1}, while the preliminary search for vector-like top partners with high BR to Ht uses a partial dataset of the same data, amounting to 14.3 fb^{-1}.

The Chapter is organized as follows: Section 5.1 and Section 5.2 present respectively the data and Monte Carlo samples used in the searches, which are in general common to both analyses with only few exceptions that are reported; Section 5.3 describes how the multi-jet background from QCD events is obtained; Section 5.4 contains a brief reminder of object definition. Finally, the two analyses are detailed in Section 5.5 and Section 5.6, which illustrate the event selection criteria, the background modeling estimation, the systematics affecting the analysis, the statistical treatment and the results.

5.1 Data sample

5.2 Monte Carlo simulated samples

5.2.1 SM processes

5.2.2 Signal samples

5.3 Multi-jet background

5.4 Object definition

5.5 Search for $T\bar{T}$ pairs decaying to $Wb + X$

5.5.1 Boosted W reconstruction

5.5.2 Control regions

5.5.3 Event selection

5.5.4

5.5.5

5.5.6 Systematics

5.6 Preliminary search for $T\bar{T}$ pairs decaying to $Ht + X$

5.6.1 Control regions

5.6.2 Event selection

5.6.3

5.6.4

5.6.5 Systematics

Chapter 6

Statistical treatment and Results

6.1 The CL_s method

6.2 Results

Conclusions

Appendix A

Appendix B

Appendix C

Search for $T\bar{T} \to Wb + X$ at $\sqrt{7}$ TeV

Bibliography

[1] J.A. Aguilar-Saavedra. Identifying top partners at LHC. *JHEP*, 0911:030, 2009.

[2] Stephen P. Martin. Extra vector-like matter and the lightest Higgs scalar boson mass in low-energy supersymmetry. *Phys.Rev.*, D81:035004, 2010.

[3] ATLAS Collaboration. The ATLAS Experiment at the CERN Large Hadron Collider. *JINST*, 3:S08003, 2008.

[4] L. Evans, P. Bryant (Eds.). LHC Machine. *JINST*, 3:S08001, 2008.

[5] CMS Collaboration. The CMS experiment at the CERN LHC. *JINST*, 3:S08004, 2008.

[6] ALICE Collaboration. The ALICE experiment at the CERN LHC. *JINST*, 3:S08002, 2008.

[7] LHCb Collaboration. The LCHb experiment at the CERN LHC. *JINST*, 3:S08005, 2008.

[8] M. Lamont. The First Years of LHC Operation for Luminosity Production. *in* Proceedings of 4th International Particle Accelerator Conference (IPAC 2013), 2013.

[9] ATLAS Collaboration.

[10] ATLAS Collaboration. Studies of the performance of the atlas detector using cosmic-ray muons. *Eur. Phys. J.*, C 71:1593, 2011.